

Chiral SPINOL-Based Pt(II) Metallacycles For Immunogenic Cell Death

Lu Zhu, Wenjing Du, Yanrong Li,* Ding Li, Wei Wei,* Jing Zhao,* and Xiuxiu Wang*

Cite This: <https://doi.org/10.1021/acs.inorgchem.3c01635>

Read Online

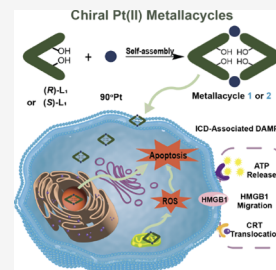
ACCESS |

Metrics & More

Article Recommendations

Supporting Information

ABSTRACT: The incorporation of chirality endows Pt(II)-based metal–organic complexes (MOCs) with unique potentials in several fields such as nonlinear optics and chiral catalysis. However, the exploration of chiral Pt(II) metallacycles in biological responses remains underdeveloped. Herein, we designed and synthesized two chiral Pt(II) metallacycles **1** and **2** via the coordination-driven self-assembly of chiral 1,1'-spirobiindane-7,7'-diol (SPINOL)-derived ligands and *cis*-Pt(PEt₃)₂(OTf)₂ (90°Pt). Their structures were well characterized by ¹H NMR, ³¹P{¹H} NMR, ESI-TOF-MS, and X-ray crystallography, and their photophysical properties were investigated by UV–vis absorption, fluorescence, and circular dichroism (CD) spectroscopies. Then, the antitumor activity of the two chiral metallacycles *in vitro* was further tested. Complexes **1** and **2** exhibited strong cytotoxicity, especially toward the A549 cells. The destruction of the mitochondrial function, the inhibition of the glutathione (GSH)/glutathione disulfide (GSSG) level, and the inactivation of superoxide dismutase (SOD) induced by complexes **1** and **2** led to the massive accumulation of reactive oxygen species (ROS). The overloaded ROS then triggered apoptotic cell death, and the release of damage-associated molecular patterns (DAMPs) further induced immunogenic cell death (ICD). To the best of our knowledge, this is the first example of Pt(II)-based metallacycles that can induce immunogenic cell death, providing a new strategy for the future design and construction of immune-modulating platinum agents in cancer therapy.



1. INTRODUCTION

Coordination-driven self-assembly is an efficient strategy for construction of diverse metal–organic complexes (MOCs).^{1–9} In the past few decades, various MOCs have been prepared via coordination and shown a potential value in chemistry,^{10–20} biomedicine,^{3,21} and materials science,^{20,22–25} among which chiral MOCs attract chemists' particular attention due to their relevance to biological functions.^{26–29} The incorporation of chirality into discrete MOCs would lead to a well-defined enzyme-like chiral pocket or functionality, which could provide an artificial chiral microenvironment. A wide range of chiral metallacycles and cages have emerged as functional materials in nonlinear optics,^{30,31} enantioselective recognition,^{32–34} asymmetric catalysis,^{35–38} and drug delivery.^{39–42} As important members of the MOC family, Pt(II)-based metallacycles and cages have been studied for cancer treatment for decades.⁴³ Classic chiral Pt(II) MOCs, such as oxaliplatin, have shown biological activity in cancer treatment. Recently, many other chiral Pt(II) MOCs have been successfully constructed,^{30,33,37,38,44–47} while their application was mainly in asymmetric catalysis, and their biological responses were less explored.

Most chiral Pt(II) MOCs generally employ axial chiral ligands, of which 1,1'-binaphthol (BINOL) was the most commonly used ligand skeleton.^{33,35,37,44,48} 1,1'-Spirobiindane-7,7'-diol (SPINOL), a superior chiral spiro skeleton with conformational rigidity and chemical robustness, has been widely employed in asymmetric catalysis.^{49–52} Except for chiral catalysis, other attempts have been made with SPINOL

derivatives. SPINOL-based phosphoric acid hosts were employed for efficient enantioselective liquid–liquid extraction of 1,2-amino-alcohols.⁵³ Aldehyde derivatives of SPINOL were used for enantioselective fluorescence imaging of free amino acids in living cells.⁵⁴ A series of tris(SPINOL)Ln^{III} complexes were found to be luminescent and chiroptically active for both circular dichroism and circularly polarized luminescence in visible and near-infrared light.⁵⁵ Unlike BINOL-derived ligands, SPINOL derivatives have rarely been reported as bridging ligands for the construction of chiral MOCs, providing a promising precursor for the design and synthesis of chiral MOCs with novel functions.

ICD is a unique form of regulated cell death (RCD) that stimulated a tumor-specific immune system as a “second hit” to the residual cancer cells, which were not killed by the original drug cytotoxicity.^{56,57} Recently, increasing efforts have been devoted to metal complexes as ICD inducers.⁵⁸ Platinum complexes have been recognized as potential candidates since oxaliplatin was reported as the first metal-based ICD inducer.⁵⁹ Ang et al. evaluated a library of Pt(II) compounds in inducing ICD, among which Pt-NHC was found to display the

Received: May 18, 2023

Scheme 1. Formation of Chiral Pt(II) Metallacycles 1 and 2 via Coordination-Driven Self-Assembly

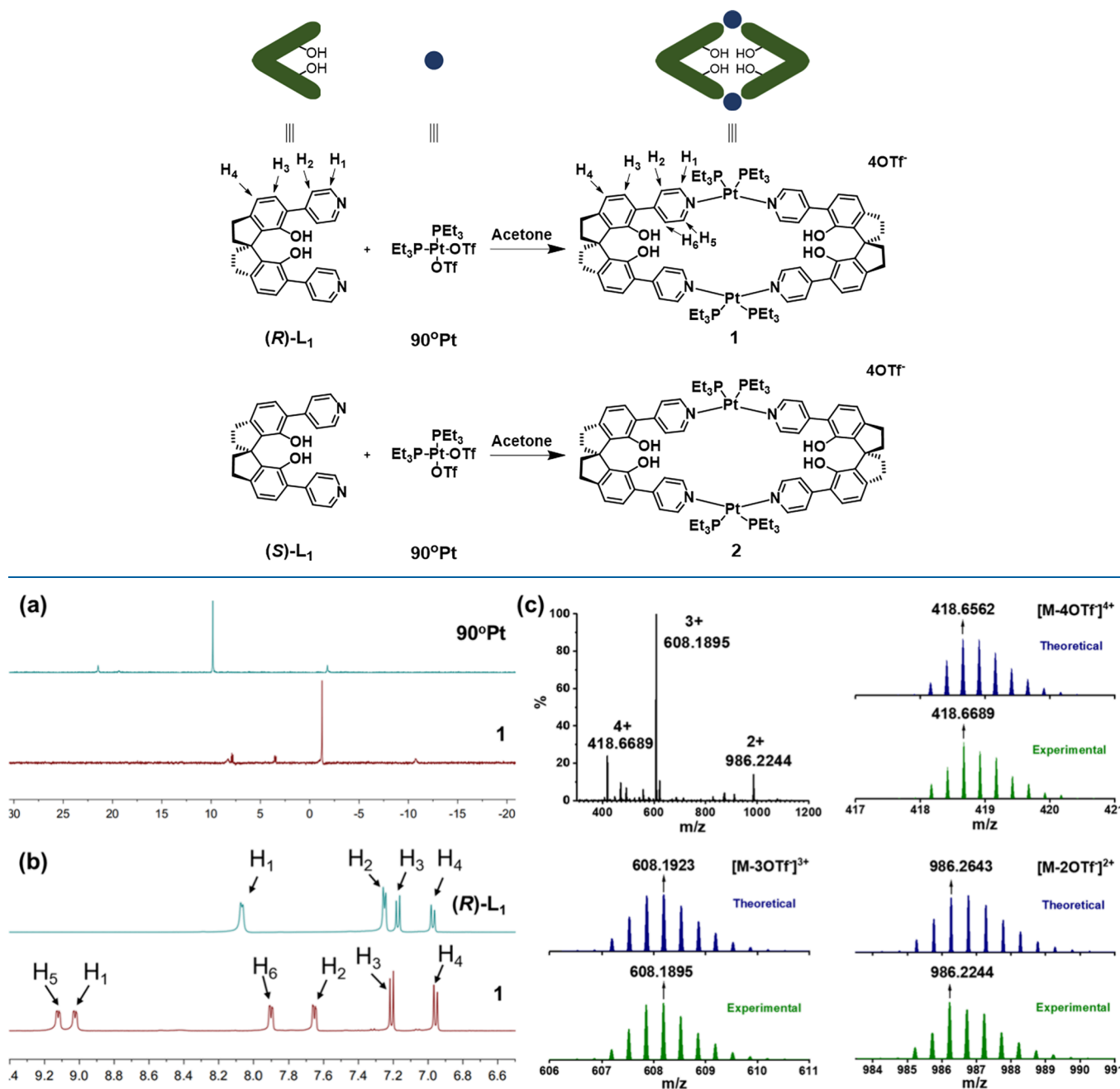


Figure 1. (a) $^{31}\text{P}\{^1\text{H}\}$ NMR spectra of 90°Pt and metallacycle 1. (b) Partial ^1H NMR spectra of $(R)\text{-L}_1$ and metallacycle 1 (400 MHz, dichloromethane- d_2 , 298 K). (c) Calculated (blue) and experimental (green) ESI-TOF-MS spectra of metallacycle 1.

characteristic hallmarks of a type II ICD inducer.⁶⁰ The nanoparticles formed by Pt-NHC and BODIPY photosensitizer via electrostatic interaction showed a strong immune response in triple-negative breast cancer cells.⁶¹ PlatinER was lately confirmed as a highly potent anticancer Pt(II) complex by inducing ERS-mediated ICD.⁶² A Pt(IV) prodrug that contains the histone deacetylase inhibitor can be easily absorbed by cancer cells and induce strong immunogenic cell death.⁶³ Liang et al. synthesized a Pt(II) complex containing an aminophosphonate ligand, which preferentially accumulated in the endoplasmic reticulum and induced strong ER stress and ROS generation, thereby inducing immune responses.⁶⁴ Artoxiplatin, a prodrug of oxaliplatin with two artesunate

molecules in the axial positions, was encapsulated by an amphiphilic polymer to form cancer nanobombs, which could amplify the ICD effect, facilitate DC maturation, and finally elicit robust antitumor immunity.⁶⁵ Nanoparticles based on an oxaliplatin-functionalized polymeric chain, an AIE photosensitizer, and cancerous tissue-targeting peptides R_8K presented a multimodal treatment by chemotherapy and photodynamic immunotherapy.⁶⁶

Herein, we first synthesized two chiral SPINOL-derived Pt(II) metallacycles 1 and 2 via coordination-driven self-assembly. The structures were well characterized by ^1H NMR, $^{31}\text{P}\{^1\text{H}\}$ NMR, ESI-TOF-MS, and single X-ray crystallography diffraction. We also studied their photophysical properties by

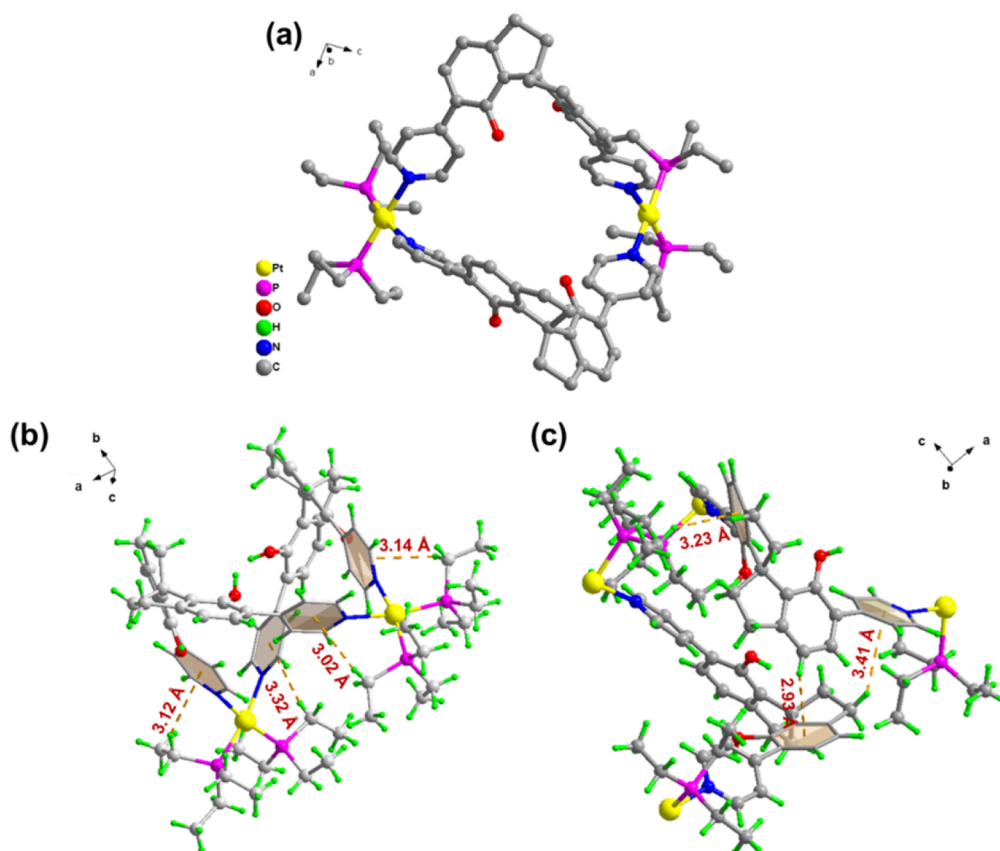


Figure 2. (a) Single-crystal structure of metallacycle **1**. (b) Intramolecular interaction of metallacycle **1**. (c) Intermolecular interaction of metallacycle **1**. (Counterions and solvent molecules are omitted for clarity.)

UV–vis absorption, fluorescence, and circular dichroism (CD) spectroscopies. Platinum-based metallacycles have been well employed as anticancer agents owing to their superior tumor antiproliferation effect;⁴³ thus, antitumor properties of two chiral metallacycles *in vitro* were further investigated. Complexes **1** and **2** exhibited strong cytotoxicity toward A549 cells. The mitochondrial dysfunction, decrease in intracellular GSH/GSSG level, and inactivation of SOD led to the massive production of ROS together. The overloaded ROS then triggered apoptotic cell death and immunogenic cell death, which was confirmed by the detection of typical hallmarks of ICD. To the best of our knowledge, this is the first example of Pt(II)-based metallacycles that can induce immunogenic cell death.

2. RESULTS AND DISCUSSION

2.1. Preparation and Characterization. As shown in Scheme S1, the 6,6'-dipyridyl substituted chiral donors (*R*)-L₁ and (*S*)-L₁ were synthesized in four steps from commercially available (*R*)-SPINOL and (*S*)-SPINOL with a total yield of 51%. The prepared (*R*)-L₁ and (*S*)-L₁ were proven to be enantiomerically pure by chiral HPLC analysis (Figure S7). Enantiotropic metallacycles **1** and **2** were obtained in over 90% yields via a two-component coordination-driven self-assembly strategy by stirring the chiral ligands (*R*)-L₁ and (*S*)-L₁ with the *cis*-Pt(PET₃)₂(OTf)₂ (90°Pt) in a molar ratio of 1:1 in acetone⁴⁴ (Scheme 1). The formation of chiral metallacycles was confirmed by multinuclear NMR spectroscopy (¹H NMR and ³¹P{¹H} NMR), electrospray ionization time-of-flight mass spectroscopy (ESI-TOF-MS), and X-ray crystallography

diffraction. Here, metallacycle **1** was selected for discussion. As depicted in Figures 1a, the ³¹P{¹H} NMR spectra of 90°Pt displayed a sharp single peak with two concomitant ¹⁹⁵Pt satellites at *d* = 21.46 and −1.80 ppm. For metallacycle **1**, two concomitant ¹⁹⁵Pt satellites are at *d* = 8.26 and −10.76 ppm, revealing the formation of a discrete, charge-separated metallacycle. After the formation of chiral metallacycles, the signals in the ³¹P{¹H} NMR spectra of **1** shifted upfield by approximately 11.09 ppm compared with that of 90°Pt. The coupling constant (*J*_{Pt–P}) of the ¹⁹⁵Pt satellites was determined to be 3792.8 Hz for metallacycle **1**. In the ¹H NMR spectra (Figure 1b), the peaks of protons on the pyridyl groups shifted downfield, indicating a decrease in electron density of the pyridine upon coordination with the Pt(II) center. Additionally, the peaks of the pyridinyl protons splintered significantly. The correlation and spatial distance between protons were analyzed by ¹H–¹H NOESY and ¹H–¹H COSY NMR, and the protons were assigned accordingly (Figure 1b and Figures S9 and S10). The ESI-TOF-MS spectra of **1** show peaks at *m/z* = 418.6689, 608.1895, and 986.2244, corresponding to the [M-4OTf]⁴⁺, [M-3OTf]³⁺, and [M-2OTf]²⁺ species (Figure 1c), which were in good agreement with the calculated theoretical values.

2.2. X-ray Crystal Analysis. The structure of metallacycle **1** in its crystalline form was characterized by X-ray crystallography diffraction. Transparent crystals of **1** suitable for crystallographic analysis were successfully obtained by diffusion of diethyl ether into the acetone solution of **1** at −20 °C. The X-ray crystal structures of **1** are shown in Figure 2, and the relevant data are listed in Tables S1 and S2. The crystal

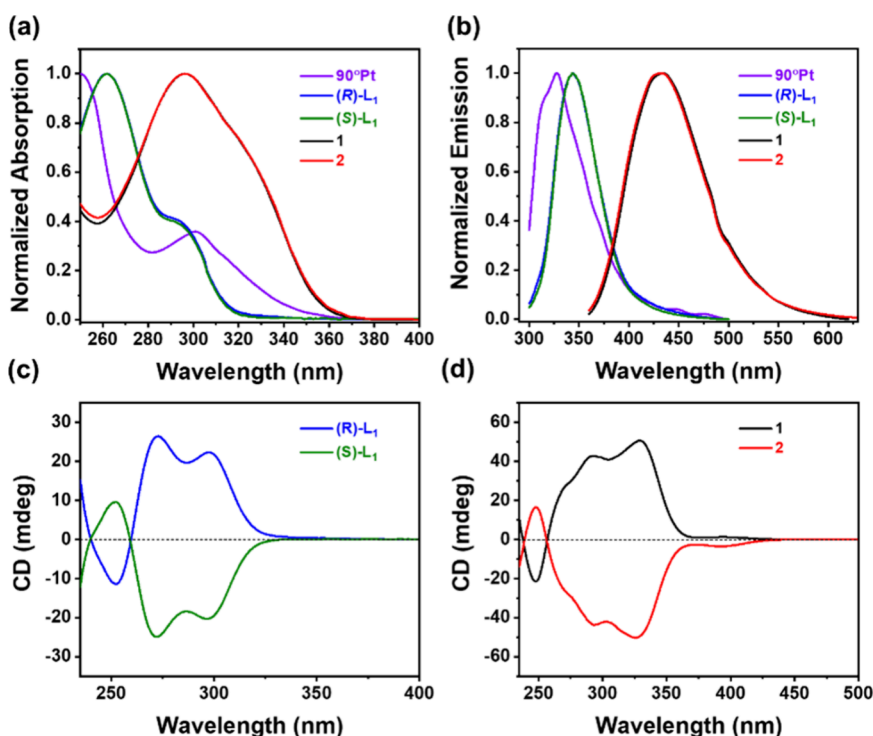


Figure 3. (a) UV–vis absorption and (b) fluorescence spectra of 90°Pt, (R)-L₁, (S)-L₁, 1, and 2. (c) CD spectra of (R)-L₁ and (S)-L₁. (d) CD spectra of 1 and 2 (dichloromethane, 2×10^{-5} M).

Table 1. IC₅₀ Values (μ M) of 90°Pt, (R)-L₁, (S)-L₁, 1, 2, and Cisplatin^a

IC ₅₀ (μ M)	A549	MG63	SiHa	MRC-5
90°Pt	41.30 \pm 2.17	31.04 \pm 4.90	91.64 \pm 6.61	98.57 \pm 4.01
(R)-L ₁	>100	>100	>100	>100
(S)-L ₁	>100	>100	>100	>100
1	4.91 \pm 0.41	7.58 \pm 0.08	29.67 \pm 2.20	30.33 \pm 1.67
2	4.73 \pm 0.45	5.61 \pm 0.32	26.42 \pm 1.09	24.22 \pm 1.67
cisplatin	11.74 \pm 2.67	27.62 \pm 7.39	11.99 \pm 0.65	11.50 \pm 2.05

^aCell viability was measured by CCK8 assay after 48 h incubation with different complexes.

phase of **1** was orthorhombic with a $P2(1)2(1)2(1)$ space group. As shown in Scheme 1 and Figure 2a, metallacycle **1** was formed via coordination of two (R)-L₁ ligands with 90°Pt acceptors with an average Pt...Pt separation of about 11.8 Å, which was balanced by OTf⁻ anions. The metallacycles were in a folded state with the N–Pt–N bite angles of $82.3 \pm 0.1^\circ$, and four coordinated atoms (N, N, P, and P) around the Pt atom adopted a nearly square-planar geometry. Extensive intramolecular CH... π interactions were found between the methylene of the triethylphosphine moiety and pyridyl (3.02–3.32 Å) (Figure 2b). **1** also interacted with the neighboring metallacycle through CH... π interactions, such as the interaction between the cyclopentyl and pyridyl of adjacent cycles (2.93–3.41 Å) (Figure 2c).

2.3. Photophysical Properties. The photophysical properties of two chiral metallacycles **1** and **2**, as well as ligands (R)-L₁ and (S)-L₁, were investigated by UV–vis absorption, fluorescence spectroscopy, and CD experiments (Figure 3). (R)-L₁ and (S)-L₁ showed strong UV absorption bands at around 260 and 293 nm. Compared with the absorption of ligands, the absorption of two metallacycles was red-shifted by 30 nm, which could be attributed to the metal coordination. **1** and **2** exhibited broad emission spectra with a peak at 432 nm. Similarly, the emission of these metallacycles

was significantly red-shifted compared to those of the corresponding ligands upon the formation of metallacycles. As depicted in Figure 3c,d, the CD spectra of chiral ligands and metallacycles in dilute dichloromethane solution presented a good mirror-image relationship with alternating positive and negative Cotton effects from 230 to 450 nm, which were consistent with their UV–vis absorption spectra. Compared with the CD signals of chiral ligands, the CD spectra of metallacycles showed a new lower energy CD signal at \sim 330 nm, which might be attributed to ligand-to-Pt(II) charge transfer and were also evidence for the formation of **1** and **2**.³⁰ The enhanced CD signals for the metallacycles were consistent with the presence of multiple ligands in chiral metal–organic complexes.

2.4. In Vitro antiproliferation Activity. The antiproliferative activity of 90°Pt, (R)-L₁, (S)-L₁, **1**, and **2**, as well as cisplatin (CDDP, positive control), was evaluated against A549 human nonsmall cell lung cancer cells, MG63 human osteosarcoma cells, SiHa human cervical squamous cell carcinoma cells, and MRC-5 human embryonic lung fibroblasts using Cell Counting Kit-8 (CCK-8) assay. It was found that chiral ligands showed little cytotoxicity toward all of the cell lines tested, and 90°Pt showed low cytotoxicity against A549 and MG63 cell lines. However, enhanced cytotoxicity was

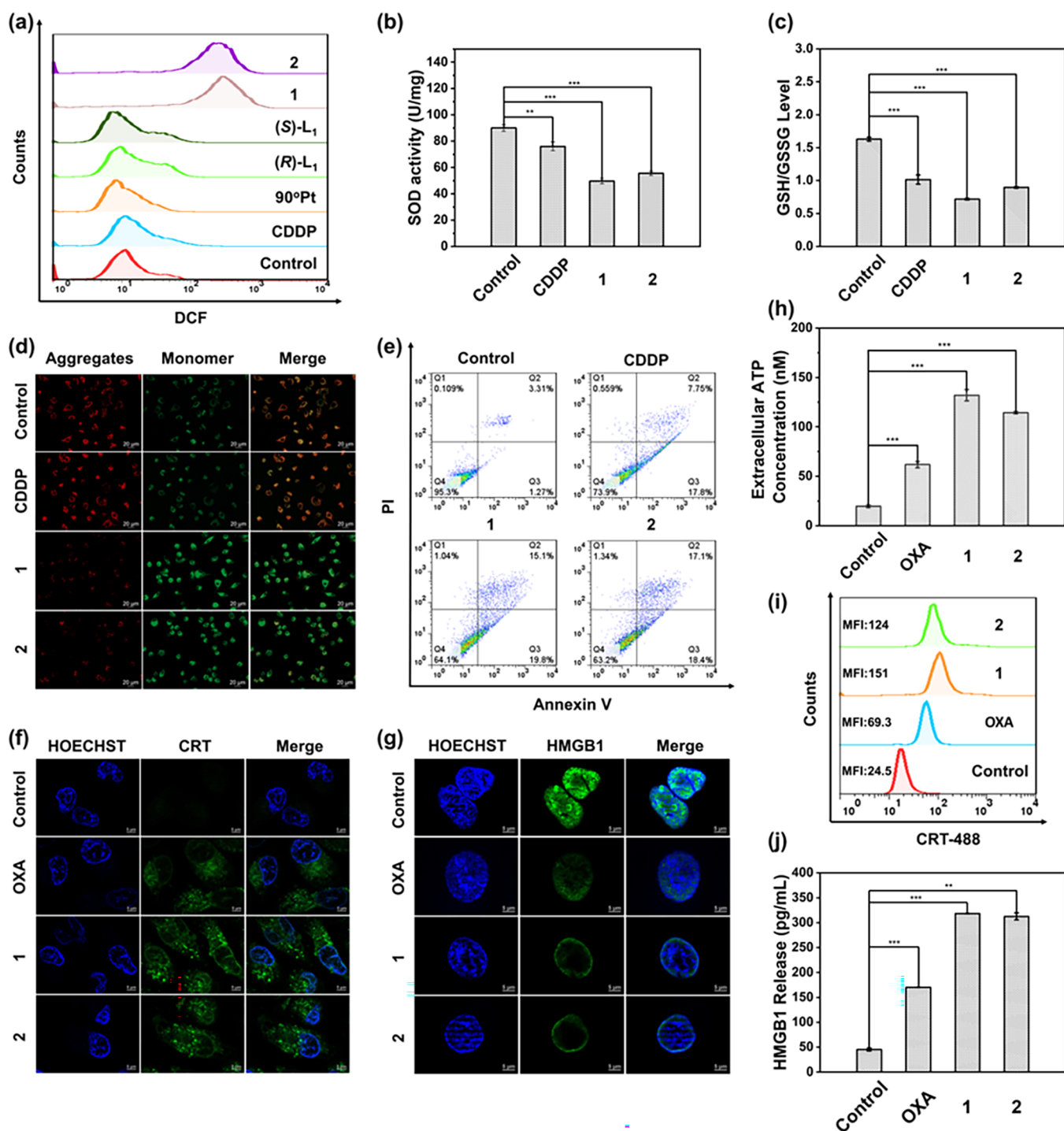


Figure 4. Mechanism analysis and ICD detection. (a) Flow cytometry analysis of ROS production of A549 cells after treatments for 24 h. (b) Intracellular SOD activity of A549 cells treated with PBS (control), CDDP, 1, and 2. (c) Intracellular GSH/GSSG level of A549 cells after treatment with PBS, CDDP, 1, and 2. (d) Mitochondrial membrane potential imaging of A549 cells with treatments via JC-1 staining. Red represents hyperpolarization, and green represents depolarization of the mitochondrial membrane potential; scale bars: 20 μm. (e) Apoptosis detection of A549 cells treated with PBS, CDDP, 1, and 2. (f) Immunofluorescence verification of calreticulin translocation to the cell membrane of A549 cells treated with PBS, OXA, 1, and 2; scale bar: 5 μm. (g) Immunofluorescence verification of HMGB1 release from the nucleus of the A549 cells treated with PBS, OXA, 1, and 2; scale bar: 5 μm. (h) Level of secreted ATP in the medium supernatant of A549 cells treated with PBS, OXA, 1, and 2. (i) Flow cytometry analysis of CRT-positive cells after treatments with PBS, OXA, 1, and 2. (j) Quantitative examination of released HMGB1 in the medium after treatments with PBS, OXA, 1, and 2 by ELISA for 24 h. Values are expressed as the mean ± SD of triplicate measurements (**p* < 0.05, ***p* < 0.01, and ****p* < 0.001).

observed once 90°Pt and chiral ligands self-assembled into metallacycles, especially for A549 and MG63 cell lines. The two mirror isomers of chiral drugs may have markedly different

biological activities, while there was no significant difference in the cytotoxicity of metallacycles 1 and 2. Metallacycle 1 exhibited the strongest inhibition against A549 cells with an

IC₅₀ value of 4.7 μM , which was much lower than that of cisplatin (ca. 11.7 μM). Notably, it was almost nontoxic to the normal cell line MRC-5 at a low concentration, indicating the superior selectivity of **1** and **2** toward cancer cells (Table 1 and Figure S12). **1** and **2** showed greater cytotoxicity than their precursors (R)-L₁ and (S)-L₁, possibly due to their better cell internalization ability, which was caused by the interaction between the positive charges of metallacycles and the negative charges on the cytomembrane.³

2.5. Cellular Uptake and Distribution. For the high anticancer efficiency of platinum metallacycles in A549 cells, we then investigated the intracellular uptake and subcellular distribution of CDDP, **1**, and **2** in A549 cells through inductively coupled plasma mass spectrometry (ICP-MS). As displayed, the intracellular uptake of **1** and **2** in A549 cells was relatively low within 12 h (Figure S13). After treatment for 24 h, the total Pt content in metallacycle-treated A549 cells was slightly lower than that of cisplatin. However, the low uptake of Pt did not affect the activity of metallacycles toward A549 cancer cells. Also, DNA damage caused by metallacycles can also be confirmed via the interaction with pUC-19 plasmid DNA *in vitro* (Figure S14). Further, the subcellular distribution of **1** was mainly in the mitochondria, while a small amount was distributed in the nucleus and endoplasmic reticulum (Table S4), which indicated that metallacycles might inhibit cell proliferation by inducing mitochondrial dysfunction.

2.6. Mitochondrial Membrane Potential (MMP, $\Delta\Psi_m$) Detection. A large amount of accumulation of **1** and **2** in mitochondria may cause mitochondrial dysfunction and lead to cell apoptosis for the crucial role of mitochondria in possessing essential physiological functions.^{67,68} We then detected the mitochondrial membrane potential (MMP, $\Delta\Psi_m$) using JC-1 staining. As indicated in Figure 4d, the green-to-red fluorescence (G/R) ratio is about 0.87 in the control group, while the G/R ratios turned out to be 4.95 and 3.65 in cells treated with **1** and **2** for 24 h, respectively. The G/R ratio increase indicated the depolarization of the mitochondria and mitochondrial dysfunction, which might contribute to the final cancer cell death. The following apoptosis detection confirmed the apoptotic cell death induced by **1** and **2** via annexin V/propidium iodide (AV/PI) costaining assay (Figure 4e).

2.7. Intramolecular ROS Production. Mitochondria are considered to be the primary site of endogenous ROS production, and mitochondrial damage directly results in the accumulation of ROS.^{67,68} The intracellular ROS level was then determined by the classic ROS probe 2,7-dichlorodihydro-fluorescein diacetate (DCFH-DA). As shown in Figure 4a and Figure S15, the intracellular ROS level increased after treatment with **1** and **2** for 12 h, and the accumulation of ROS was particularly obvious in the 24 h experimental group. Meanwhile, no ROS accumulation can be observed in cells treated with 90°Pt or chiral ligands. Furthermore, cellular imaging via DCFH-DA and MitoTracker Red staining revealed that mitochondria are the subcellular location of ROS production (Figure S16). In addition, the intracellular glutathione (GSH)/glutathione disulfide (GSSG) and superoxide dismutase (SOD) activities were reduced by metallacycles (Figure 4b,c). These decrease in GSH/GSSG levels and SOD activity weakened scavenging capability to ROS, further leading to the accumulation of intracellular ROS.

2.8. Release of ICD-Associated DAMPs. Considering the subcellular distribution of metallacycles in the endoplasmic reticulum (ER, Table S4) and the massive accumulation of

ROS, we next speculated that ROS-mediated ER stress was most likely stimulated by metallacycles in cancer cells. As cancer cells may respond to ROS-mediated ER stress by releasing a combination of damage-associated molecular patterns (DAMPs) from dying cancer cells as “danger” signals, which are subsequently recognized by respective pattern recognition receptors and further active intracellular ICD pathways,⁶⁹ we next detected the possible release of DAMPs in dying cancer cells. As a known platinum-based ICD inducer, oxaliplatin was selected as a positive control drug for ICD detection. A representative hallmark of ICD is the exposure of calreticulin (CRT), which is a Ca²⁺-binding chaperon protein present in the ER lumen and translocates to the plasma membrane during early apoptosis and serves as an “eat-me” signal.⁶⁹ First, the translocation of CRT from the ER lumen to the cell membrane in the OXA, **1**, and **2** treatment groups could be observed via immunofluorescence analysis, and **1** and **2** induced a higher CRT expression than the OXA by flow cytometry assay (Figure 4f,i). In addition, after metallacycle treatment, the secretion of extracellular ATP increased 5-fold when compared with the control group (Figure 4h). The efflux of high mobility group box 1 protein (HMGB1) from the nucleus, another critical indicator of ICD, was also monitored via immunofluorescence analysis. As shown in Figure 4g, in nontreated A549 cells, HMGB1 protein was mainly located in the nucleus, and after the treatment of metallacycles, most of the nuclear HMGB1 protein migrated to the cytoplasm. The released HMGB1 in the medium was also quantified by the enzyme-linked immunosorbent assay (ELISA). As clearly indicated in Figure 4j, the release of HMGB1 induced by **1** and **2** was much higher than that of OXA. Altogether, the translocation and exposure of CRT, the secretion of ATP, and the release of HMGB1 confirmed the immunogenic cell death induced by metallacycles. Notably, this ICD effect was more evident than the reported oxaliplatin as an ICD inducer.

3. CONCLUSIONS

In summary, two chiral metallacycles based on SPINOL derivatives were constructed via coordination-driven self-assembly. Their structures were well characterized by ¹H NMR, ³¹P{¹H} NMR, ESI-TOF-MS, and X-ray crystallography, and the photophysical properties were investigated by multiple spectroscopies. The antitumor properties of two metallacycles *in vitro* were tested and confirmed to be stronger type I ICD inducers than oxaliplatin. The accumulation of these two metallacycles in mitochondria and the inhibition of the GSH/GSSG level and the inactivation of SOD led to massive accumulation of ROS. The overloaded ROS then triggered apoptotic cell death and immunogenic cell death, which was confirmed by the hallmarks of translocation of CRT, the release of ATP, and migration of HMGB1 in A549 cancer cells. This study first developed a pair of chiral dinuclear Pt(II) metallacycles as effective ICD inducers, which represented a great attempt for the exploration of immune-modulated Pt(II) complexes, providing a new structure-design strategy for future immune-modulating platinum agents in cancer therapy.

■ ASSOCIATED CONTENT

Supporting Information

The Supporting Information is available free of charge at <https://pubs.acs.org/doi/10.1021/acs.inorgchem.3c01635>.

General procedures, analysis data for SINOL derivatives and metallacycles, and additional biological experimental data (PDF)

Accession Codes

CCDC 2260747 contains the supplementary crystallographic data for this paper. These data can be obtained free of charge via www.ccdc.cam.ac.uk/data_request/cif, or by emailing data_request@ccdc.cam.ac.uk, or by contacting The Cambridge Crystallographic Data Centre, 12 Union Road, Cambridge CB2 1EZ, UK; fax: +44 1223 336033.

AUTHOR INFORMATION

Corresponding Authors

Yanrong Li – Chemistry and Biomedicine Innovation Center (ChemBIC), State Key Laboratory of Coordination Chemistry, School of Chemistry and Chemical Engineering, Nanjing University, Nanjing 210023, China; Department of Chemistry, Boston College, Chestnut Hill, Massachusetts 02467, United States; orcid.org/0000-0001-5180-1965; Email: dg1524042@smail.nju.edu.cn

Wei Wei – School of Life Sciences and Chemistry and Biomedicine Innovation Center (ChemBIC), State Key Laboratory of Coordination Chemistry, School of Chemistry and Chemical Engineering, Nanjing University, Nanjing 210023, China; Sino-Danish Ecolife Science Industrial Incubator, Nanchuang (Jiangsu) Institute of Chemistry and Health, Nanjing 210000, China; orcid.org/0000-0003-0845-0527; Email: weiwei@nju.edu.cn

Jing Zhao – Chemistry and Biomedicine Innovation Center (ChemBIC), State Key Laboratory of Coordination Chemistry, School of Chemistry and Chemical Engineering, Nanjing University, Nanjing 210023, China; Sino-Danish Ecolife Science Industrial Incubator, Nanchuang (Jiangsu) Institute of Chemistry and Health, Nanjing 210000, China; orcid.org/0000-0001-5177-5699; Email: jingzhao@nju.edu.cn

Xiuxiu Wang – Chemistry and Biomedicine Innovation Center (ChemBIC), State Key Laboratory of Coordination Chemistry, School of Chemistry and Chemical Engineering, Nanjing University, Nanjing 210023, China; Email: wangxiuxiu@nju.edu.cn

Authors

Lu Zhu – School of Life Sciences, Nanjing University, Nanjing 210023, China

Wenjing Du – Chemistry and Biomedicine Innovation Center (ChemBIC), State Key Laboratory of Coordination Chemistry, School of Chemistry and Chemical Engineering, Nanjing University, Nanjing 210023, China

Ding Li – Chemistry and Biomedicine Innovation Center (ChemBIC), State Key Laboratory of Coordination Chemistry, School of Chemistry and Chemical Engineering, Nanjing University, Nanjing 210023, China

Complete contact information is available at:

<https://pubs.acs.org/10.1021/acs.inorgchem.3c01635>

Notes

The authors declare no competing financial interest.

ACKNOWLEDGMENTS

This work was supported by the National Natural Science Foundation of China (22207053, 22025701, 22177048, and

22101129), the Natural Science Foundation of Jiangsu Province (BK20220764 and BK20202004), and 2021 Strategic Research Project of the Science and Technology Commission of the Ministry of Education of China.

REFERENCES

- (1) Chakrabarty, R.; Mukherjee, P. S.; Stang, P. J. Supramolecular Coordination: Self-Assembly of Finite Two- and Three-Dimensional Ensembles. *Chem. Rev.* **2011**, *111*, 6810–6918.
- (2) Cook, T. R.; Stang, P. J. Recent Developments in the Preparation and Chemistry of Metallacycles and Metallacages via Coordination. *Chem. Rev.* **2015**, *115*, 7001–7045.
- (3) Sepehrpour, H.; Fu, W.; Sun, Y.; Stang, P. J. Biomedically Relevant Self-Assembled Metallacycles and Metallacages. *J. Am. Chem. Soc.* **2019**, *141*, 14005–14020.
- (4) Sun, Y.; Chen, C.; Liu, J.; Stang, P. J. Recent Developments in the Construction and Applications of Platinum-Based Metallacycles and Metallacages via Coordination. *Chem. Soc. Rev.* **2020**, *49*, 3889–3919.
- (5) Rizzuto, F. J.; von Krbek, L. K. S.; Nitschke, J. R. Strategies for Binding Multiple Guests in Metal-Organic Cages. *Nat. Rev. Chem.* **2019**, *3*, 204–222.
- (6) Tang, J.-H.; Zhong, Y.-W. Anthracene-Containing Metallacycles and Metallacages: Structures, Properties, and Applications. *Inorganics* **2022**, *10*, 88.
- (7) Percastegui, E. G.; Jancik, V. Coordination-Driven Assemblies Based on Meso-Substituted Porphyrins: Metal-Organic Cages and a New Type of Meso-Metallaporphyrin Macrocycles. *Coord. Chem. Rev.* **2020**, *407*, No. 213165.
- (8) Wang, M.-F.; Mi, Y.; Hu, F.-L.; Niu, Z.; Yin, X.-H.; Huang, Q.; Wang, H.-F.; Lang, J.-P. Coordination-Driven Stereospecific Control Strategy for Pure Cycloisomers in Solid-State Diene Photocycloaddition. *J. Am. Chem. Soc.* **2020**, *142*, 700–704.
- (9) Zhang, D.; Ronson, T. K.; Nitschke, J. R. Functional Capsules via Subcomponent Self-Assembly. *Acc. Chem. Res.* **2018**, *51*, 2423–2436.
- (10) Yan, X.; Wang, H.; Hauke, C. E.; Cook, T. R.; Wang, M.; Saha, M. L.; Zhou, Z.; Zhang, M.; Li, X.; Huang, F.; Stang, P. J. A Suite of Tetraphenylethylene-Based Discrete Organoplatinum(II) Metallacycles: Controllable Structure and Stoichiometry, Aggregation-Induced Emission, and Nitroaromatics Sensing. *J. Am. Chem. Soc.* **2015**, *137*, 15276–15286.
- (11) Saha, R.; Devaraj, A.; Bhattacharyya, S.; Das, S.; Zangrando, E.; Mukherjee, P. S. Unusual Behavior of Donor-Acceptor Stenhouse Adducts in Confined Space of a Water-Soluble Pd-8(II) Molecular Vessel. *J. Am. Chem. Soc.* **2019**, *141*, 8638–8645.
- (12) Acharyya, K.; Bhattacharyya, S.; Sepehrpour, H.; Chakraborty, S.; Lu, S.; Shi, B.; Li, X.; Mukherjee, P. S.; Stang, P. J. Self-Assembled Fluorescent Pt(II) Metallacycles as Artificial Light-Harvesting Systems. *J. Am. Chem. Soc.* **2019**, *141*, 14565–14569.
- (13) Zhang, D.; Ronson, T. K.; Lavendomme, R.; Nitschke, J. R. Selective Separation of Polyaromatic Hydrocarbons by Phase Transfer of Coordination Cages. *J. Am. Chem. Soc.* **2019**, *141*, 18949–18953.
- (14) Li, Y.; Rajasree, S. S.; Lee, G. Y.; Yu, J.; Tang, J.-H.; Ni, R.; Li, G.; Houk, K. N.; Deria, P.; Stang, P. J. Anthracene-Triphenylamine-Based Platinum(II) Metallacages as Synthetic Light-Harvesting Assembly. *J. Am. Chem. Soc.* **2021**, *143*, 2908–2919.
- (15) Zhang, S.; Ma, L.; Ma, W.; Chen, L.; Gao, K.; Yu, S.; Zhang, M.; Zhang, L.; He, G. Selenoviolgen-Appendant Metallacycles with Highly Stable Radical Cations and Long-Lived Charge Separation States for Electrochromism and Photocatalysis. *Angew. Chem., Int. Ed.* **2022**, *61*, No. e202209054.
- (16) Ward, M. D.; Hunter, C. A.; Williams, N. H. Coordination Cages Based on Bis(pyrazolylpyridine) Ligands: Structures, Dynamic Behavior, Guest Binding, and Catalysis. *Acc. Chem. Res.* **2018**, *51*, 2073–2082.

- (17) Hong, C. M.; Bergman, R. G.; Raymond, K. N.; Toste, F. D. Self-Assembled Tetrahedral Hosts as Supramolecular Catalysts. *Acc. Chem. Res.* **2018**, *51*, 2447–2455.
- (18) Jongkind, L. J.; Caumes, X.; Hartendorp, A. P. T.; Reek, J. N. H. Ligand Template Strategies for Catalyst Encapsulation. *Acc. Chem. Res.* **2018**, *51*, 2115–2128.
- (19) Wu, G.-Y.; Chen, L.-J.; Xu, L.; Zhao, X.-L.; Yang, H.-B. Construction of Supramolecular Hexagonal Metallacycles via Coordination-Driven Self-Assembly: Structure, Properties and Application. *Coord. Chem. Rev.* **2018**, *369*, 39–75.
- (20) Jansze, S. M.; Severin, K. Clathrochelate Metalloligands in Supramolecular Chemistry and Materials Science. *Acc. Chem. Res.* **2018**, *51*, 2139–2147.
- (21) Cook, T. R.; Vajpayee, V.; Lee, M. H.; Stang, P. J.; Chi, K.-W. Biomedical and Biochemical Applications of Self-Assembled Metallacycles and Metallacages. *Acc. Chem. Res.* **2013**, *46*, 2464–2474.
- (22) Chen, L.-J.; Yang, H.-B. Construction of Stimuli-Responsive Functional Materials via Hierarchical Self-Assembly Involving Coordination Interactions. *Acc. Chem. Res.* **2018**, *51*, 2699–2710.
- (23) Sun, Y.; Chen, C.; Stang, P. J. Soft Materials with Diverse Suprastructures via the Self-Assembly of Metal-Organic Complexes. *Acc. Chem. Res.* **2019**, *52*, 802–817.
- (24) Li, M.; Chen, L.-J.; Cai, Y.; Luo, Q.; Li, W.; Yang, H.-B.; Tian, H.; Zhu, W.-H. Light-Driven Chiral Switching of Supramolecular Metallacycles with Photoreversibility. *Chem.* **2019**, *5*, 634–648.
- (25) Gao, K.; Feng, Q.; Zhang, Z.; Zhang, R.; Hou, Y.; Mu, C.; Li, X.; Zhang, M. Emissive Metallacage-Cored Polyurethanes with Self-Healing and Shape Memory Properties. *Angew. Chem., Int. Ed.* **2022**, *61*, No. e202209958.
- (26) Hembury, G. A.; Borovkov, V. V.; Inoue, Y. Chirality-Sensing Supramolecular Systems. *Angew. Chem., Int. Ed.* **2022**, *61*, No. e202209958, DOI: 10.1021/cr050005k.
- (27) Cantekin, S.; Balkenende, D. W. R.; Smulders, M. M. J.; Palmans, A. R. A.; Meijer, E. W. The Effect of Isotopic Substitution on the Chirality of a Self-Assembled Helix. *Nat. Chem.* **2011**, *3*, 42–46.
- (28) Bai, C.; Liu, M. From Chemistry to Nanoscience: Not Just a Matter of Size. *Angew. Chem., Int. Ed.* **2013**, *52*, 2678–2683.
- (29) Wang, Y.; Xu, J.; Wang, Y.; Chen, H. Emerging Chirality in Nanoscience. *Chem. Soc. Rev.* **2013**, *42* (7), 2930–2962.
- (30) Zhu, H.; Li, Q.; Shi, B.; Xing, H.; Sun, Y.; Lu, S.; Shangquan, L.; Li, X.; Huang, F.; Stang, P. J. Formation of Planar Chiral Platinum Triangles via Pillar[5]arene for Circularly Polarized Luminescence. *J. Am. Chem. Soc.* **2020**, *142*, 17340–17345.
- (31) Huo, G.-F.; Tu, Q.; Hu, Y.-X.; Jiang, B.; Zhou, Q.-F.; Niu, Y.; Zhao, X.; Ding, H.-M.; Wen, J.; Yin, G.-Q.; Shi, X.-L.; Xu, L. Amplified Circularly Polarized Luminescence Promoted by Hierarchical Self-Assembly Involving Pt^{II}-Pt interactions. *Sci. China Mater.* **2022**, *65*, 469–476.
- (32) Zhang, L.; Liu, H.; Yuan, G.; Han, Y.-F. Chiral Coordination Metallacycles/Metallacages for Enantioselective Recognition and Separation. *Chin. J. Chem.* **2021**, *39*, 2273–2286.
- (33) Lee, S. J.; Lin, W. B. A Chiral Molecular Square with Metallo-Corners for Enantioselective Sensing. *J. Am. Chem. Soc.* **2002**, *124*, 4554–4555.
- (34) Pan, M.; Wu, K.; Zhang, J.-H.; Su, C.-Y. Chiral Metal-Organic Cages/Containers (MOCs): From Structural and Stereochemical Design to Applications. *Coord. Chem. Rev.* **2019**, *378*, 333–349.
- (35) Lee, S. J.; Hu, A. G.; Lin, W. B. First Chiral Organometallic Triangle for Asymmetric Catalysis. *J. Am. Chem. Soc.* **2002**, *124*, 12948–12949.
- (36) Cheng, K.-Y.; Wang, S.-C.; Chen, Y.-S.; Chan, Y.-T. Self-Assembly and Catalytic Reactivity of BINOL-Bridged Bis(phenanthroline) Metallocomplexes. *Inorg. Chem.* **2018**, *57*, 3559–3567.
- (37) Hong, T.; Zhang, Z.; Sun, Y.; Tao, J.-J.; Tang, J.-D.; Xie, C.; Wang, M.; Chen, F.; Xie, S.-S.; Li, S.; Stang, P. J. Chiral Metallacycles as Catalysts for Asymmetric Conjugate Addition of Styrylboronic Acids to α,β -Enones. *J. Am. Chem. Soc.* **2020**, *142*, 10244–10249.
- (38) Chu, D.; Gong, W.; Jiang, H.; Tang, X.; Cui, Y.; Liu, Y. Boosting Enantioselectivity of Chiral Molecular Catalysts with Supramolecular Metal-Organic Cages. *CCS Chem.* **2022**, *4*, 1180–1189.
- (39) Schmitt, F.; Freudenreich, J.; Barry, N. P. E.; Juillerat-Jeanneret, L.; Suess-Fink, G.; Therrien, B. Organometallic Cages as Vehicles for Intracellular Release of Photosensitizers. *J. Am. Chem. Soc.* **2012**, *134*, 754–757.
- (40) Zheng, Y.-R.; Suntharalingam, K.; Johnstone, T. C.; Lippard, S. J. Encapsulation of Pt(IV) Prodrugs within a Pt(II) Cage for Drug Delivery. *Chem. Sci.* **2015**, *6*, 1189–1193.
- (41) Han, J.; Raeder, A. F. B.; Reichart, F.; Aikman, B.; Wenzel, M. N.; Woods, B.; Weinmueller, M.; Ludwig, B. S.; Sturup, S.; Groothuis, G. M. M.; Permentier, H. P.; Bischoff, R.; Kessler, H.; Horvatovich, P.; Casini, A. Bioconjugation of Supramolecular Metallacages to Integrin Ligands for Targeted Delivery of Cisplatin. *Bioconjugate Chem.* **2018**, *29*, 3856–3865.
- (42) Yue, Z.; Wang, H.; Li, Y.; Qin, Y.; Xu, L.; Bowers, D. J.; Gangoda, M.; Li, X.; Yang, H.-B.; Zheng, Y.-R. Coordination-Driven Self-Assembly of a Pt(IV) Prodrug-Conjugated Supramolecular Hexagon. *Chem. Commun.* **2018**, *54*, 731–734.
- (43) Tuo, W.; Xu, Y.; Fan, Y.; Li, J.; Qiu, M.; Xiong, X.; Li, X.; Sun, Y. Biomedical Applications of Pt(II) Metallacycle/Metallacage-Based Agents: From Mono-Chemotherapy to Versatile Imaging Contrasts and Theranostic Platforms. *Coord. Chem. Rev.* **2021**, *443*, No. 214017.
- (44) Ye, Y.; Cook, T. R.; Wang, S.-P.; Wu, J.; Li, S.; Stang, P. J. Self-Assembly of Chiral Metallacycles and Metallacages from a Directionally Adaptable BINOL-Derived Donor. *J. Am. Chem. Soc.* **2015**, *137*, 11896–11899.
- (45) Lee, S. J.; Kim, J. S.; Lin, W. B. Chiral Molecular Squares Based on Angular Bipyridines: Self-Assembly, Characterization, and Photo-physical Properties. *Inorg. Chem.* **2004**, *43*, 6579–6588.
- (46) Ou-Yang, J.-K.; Zhang, Y.-Y.; He, M.-L.; Li, J.-T.; Li, X.; Zhao, X.-L.; Wang, C.-H.; Yu, Y.; Wang, D.-X.; Xu, L.; Yang, H.-B. Unexpected Self-Assembly of Chiral Triangles from 90 degrees Chiral Di-Pt(II) Acceptors. *Org. Lett.* **2014**, *16*, 664–667.
- (47) Tan, C.; Jiao, J.; Li, Z.; Liu, Y.; Han, X.; Cui, Y. Design and Assembly of a Chiral Metallosalen-Based Octahedral Coordination Cage for Supramolecular Asymmetric Catalysis. *Angew. Chem., Int. Ed.* **2018**, *57*, 2085–2090.
- (48) Ramakrishna, E.; Tang, J.-D.; Tao, J.-J.; Fang, Q.; Zhang, Z.; Huang, J.; Li, S. Self-Assembly of Chiral BINOL Cages via Imine Condensation. *Chem. Commun.* **2021**, *57*, 9088–9091.
- (49) Wang, Y.; Wang, S.; Shan, W.; Shao, Z. Direct Asymmetric N-propargylation of Indoles and Carbazoles Catalyzed by Lithium SPINOL Phosphate. *Nat. Commun.* **2020**, *11*, 226.
- (50) Lai, J.; Fianchini, M.; Pericas, M. A. Development of Immobilized SPINOL-Derived Chiral Phosphoric Acids for Catalytic Continuous Flow Processes. Use in the Catalytic Desymmetrization of 3,3-Disubstituted Oxetanes. *ACS Catal.* **2020**, *10*, 14971–14983.
- (51) Rahman, A.; Lin, X. Development and Application of Chiral Spirocyclic Phosphoric Acids in Asymmetric Catalysis. *Org. Biomol. Chem.* **2018**, *16*, 4753–4777.
- (52) Yin, L.; Xing, J.; Wang, Y.; Shen, Y.; Lu, T.; Hayashi, T.; Dou, X. Enantioselective Synthesis of 3,3'-Diaryl-SPINOLs: Rhodium-Catalyzed Asymmetric Arylation/BF₃-Promoted Spirocyclization Sequence. *Angew. Chem., Int. Ed.* **2019**, *58*, 2474–2478.
- (53) Pinxterhuis, E. B.; Gualtierotti, J.-B.; Heeres, H. J.; de Vries, J. G.; Feringa, B. L. Highly Efficient Enantioselective Liquid-Liquid Extraction of 1,2-Amino-Alcohols Using SPINOL Based Phosphoric Acid Hosts. *Chem. Sci.* **2017**, *8*, 6409–6418.
- (54) Zeng, C.; Zhang, X.; Pu, L. Enantioselective Fluorescent Imaging of Free Amino Acids in Living Cells. *Chem. Eur. J.* **2017**, *23*, 2432–2438.
- (55) Willis, B.-A. N.; Schnable, D.; Schley, N. D.; Ung, G. Spinolate Lanthanide Complexes for High Circularly Polarized Luminescence Metrics in the Visible and Near-Infrared. *J. Am. Chem. Soc.* **2022**, *144*, 22421–22425.

- (56) Kroemer, G.; Galluzzi, L.; Kepp, O.; Zitvogel, L. Immunogenic Cell Death in Cancer Therapy. *Annu. Rev. Immunol.* **2013**, *31*, 51–72.
- (57) Garg, A. D.; Dudek-Peric, A. M.; Romano, E.; Agostinis, P. Immunogenic Cell Death. *Int. J. Dev. Biol.* **2015**, *59*, 131–140.
- (58) Zhang, L.; Montesdeoca, N.; Karges, J.; Xiao, H. Immunogenic Cell Death Inducing Metal Complexes for Cancer Therapy. *Angew. Chem., Int. Ed.* **2023**, *62*, No. e202300662.
- (59) Tesniere, A.; Schlemmer, F.; Boige, V.; Kepp, O.; Martins, I.; Ghiringhelli, F.; Aymeric, L.; Michaud, M.; Apetoh, L.; Barault, L.; Mendiboure, J.; Pignon, J. P.; Jooste, V.; van Endert, P.; Ducreux, M.; Zitvogel, L.; Piard, F.; Kroemer, G. Immunogenic Death of Colon Cancer Cells Treated with Oxaliplatin. *Oncogene* **2010**, *29*, 482–491.
- (60) Wong, D. Y. Q.; Ong, W. W. F.; Ang, W. H. Induction of Immunogenic Cell Death by Chemotherapeutic Platinum Complexes. *Angew. Chem., Int. Ed.* **2015**, *54*, 6483–6487.
- (61) Wang, B.; Tang, D.; Karges, J.; Cui, M.; Xiao, H. A NIR-II Fluorescent PolyBodipy Delivering Cationic Pt-NHC with Type II Immunogenic Cell Death for Combined Chemotherapy and Photodynamic Immunotherapy. *Adv. Funct. Mater.* **2023**, *33*, 2214824.
- (62) Tham, M. J. R.; Babak, M. V.; Ang, W. H. PlatinER: A Highly Potent Anticancer Platinum(II) Complex that Induces Endoplasmic Reticulum Stress Driven Immunogenic Cell Death. *Angew. Chem., Int. Ed.* **2020**, *59*, 19070–19078.
- (63) Sabbatini, M.; Zanellato, I.; Ravera, M.; Gabano, E.; Perin, E.; Rangone, B.; Osella, D. Pt(IV) Bifunctional Prodrug Containing 2-(2-Propynyl)octanoato Axial Ligand: Induction of Immunogenic Cell Death on Colon Cancer. *J. Med. Chem.* **2019**, *62*, 3395–3406.
- (64) Huang, K.-B.; Wang, F.-Y.; Feng, H.-W.; Luo, H.; Long, Y.; Zou, T.; Chan, A. S. C.; Liu, R.; Zou, H.; Chen, Z.-F.; Liu, Y.-C.; Liu, Y.-N.; Liang, H. An Aminophosphonate Ester Ligand-Containing Platinum(II) Complex Induces Potent Immunogenic Cell Death in Vitro and Elicits Effective Anti-tumour Immune Responses in Vivo. *Chem. Commun.* **2019**, *55*, 13066–13069.
- (65) Gao, Y.; Zhang, H.; Tang, L.; Li, F.; Yang, L.; Xiao, H.; Karges, J.; Huang, W.; Zhang, W.; Liu, C. Cancer nanobombs Delivering Artoxin with a Polyigniter Bearing Hydrophobic Ferrocene Units Upregulate PD-L1 Expression and Stimulate Stronger Anticancer Immunity. *Adv. Sci.* **2023**, 2300806.
- (66) Wei, D.; Huang, Y.; Wang, B.; Ma, L.; Karges, J.; Xiao, H. Photo-Reduction with NIR Light of Nucleus-Targeting Pt^{IV} Nanoparticles for Combined Tumor-Targeted Chemotherapy and Photodynamic Immunotherapy. *Angew Chem Int Ed* **2022**, *61*, No. e202201486.
- (67) Kuznetsov, A. V.; Margreiter, R.; Ausserlechner, M. J.; Hagenbuchner, J. The Complex Interplay between Mitochondria, ROS and Entire Cellular Metabolism. *Antioxidants* **2022**, *11*, 1995.
- (68) Yang, Y.; Karakhanova, S.; Hartwig, W.; D'Haese, J. G.; Philippov, P. P.; Werner, J.; Bazhin, A. V. Mitochondria and Mitochondrial ROS in Cancer: Novel Targets for Anticancer Therapy. *J. Cell. Physiol.* **2016**, *231*, 2570–2581.
- (69) Sen, S.; Won, M.; Levine, M. S.; Noh, Y.; Sedgwick, A. C.; Kim, J. S.; Sessler, J. L.; Arambula, J. F. Metal-Based Anticancer Agents as Immunogenic Cell Death Inducers: the Past, Present, and Future. *Chem. Soc. Rev.* **2022**, *51*, 1212–1233.